Focused blind deconvolution of interferometric Green's functions

Pawan Bharadwaj*, Laurent Demanet, and Aimé Fournier, Massachusetts Institute of Technology

SUMMARY

We detail a novel multichannel blind deconvolution (BD) algorithm that extracts the cross-correlated or interferometric Green's functions from the records due to a single noisy source. In this framework, we perform a least-squares fit of the cross-correlated records, rather than the raw records, which greatly reduces the indeterminacy inherent to traditional BD methods. To resolve the remaining degrees of freedom, we seek a first approximation where the Green's functions are "maximally white", and relax this requirement as the iterations progress. This requirement is encoded as the focusing near zero lag of the energy of the auto-correlated Green's functions, hence we call the method focused blind deconvolution (FBD). We demonstrate the benefits of FBD using synthetic seismic-while-drilling experiments to look around and ahead of a bore-hole. Here, the noise due to the operation of the drill bit is not directly usable for reflection imaging, but FBD can provide the processing needed to extract the noise signature without unrealistically assuming the drill noise to be uncorrelated. The interferometric Green's functions obtained from FBD can either be directly imaged or further processed to output the usual subsurface Green's functions. Note that FBD is designed for an acquisition where the noise is recorded for a longer time period than the propagation time of the seismic waves e.g., as could be done during normal drilling operations. Traditional seismic imaging may now be augmented by added information around and ahead of the drill bit, potentially allowing less frequent traditional surveys.

INTRODUCTION

There are situations where seismic experiments are to be performed in environments with a noisy source. The source generates unknown, noisy signals; one fails to dependably isolate these signals despite deploying an attached receiver. For example, the exact signature of the operating drill bit in a bore-hole environment cannot be recorded (Haldorsen et al., 1995; Aminzadeh and Dasgupta, 2013). Imaging of these noisy-source signals is only possible when they are analyzed to discover the subsurface Green's functions. This is the subject of seismic interferometry (Schuster et al., 2004; Snieder, 2004; Shapiro et al., 2005; Wapenaar et al., 2006; Curtis et al., 2006; Schuster, 2009), where the cross-correlation between the records at two receivers is treated as a proxy for the cross-correlated or *interferometric* Green's function. A summation on the interferometric Green's functions over various noisy sources, evenly distributed in space, will result in the Green's functions due to a *virtual source* at one of the receivers (Wapenaar and Fokkema, 2006). In the absence of multiple evenly distributed noisy sources, the interferometric Green's functions can still be directly used for imaging (Claerbout, 1968; Draganov et al., 2006; Borcea et al., 2006; Demanet and Jugnon, 2017; Vidal et al., 2014), although this requires knowledge of the source signature. In the present work neither an even distribution of the noisy sources, nor knowledge of the source signature is assumed.

We assume that the recorded seismic traces can be modeled as the output of a linear system that convolves (denoted by $*$) a seismic source (with excitation $s(t)$ at time t) with the earth's impulse response (Robinson and Treitel, 1980). Denote the signal record at the ith receiver by $d_i(t)$ and temporal cross-correlation by $\otimes$, so that the observed

$$d_{ij}(t) = [d_i \otimes d_j](t) = [s_{\text{a}} * g_{ij}](t), \tag{1}$$

that is, the goal of interferometry, construction of the interferometric Green's functions $g_{ij} = g_i \otimes g_j$ given $d_{ij}(t)$, is impeded by the auto-correlation $s_{\text{a}} = s \otimes s$ of the source. Here, $g_i(t)$ is the "i^{th} Green's function" i.e., the unique Green's function $g(\vec{x}, t)$ evaluated at the receiver location $\vec{x}_i$. In a situation with a zero-mean white noisy source, the d_{ij} would be precisely proportional to g_{ij}; but this is not at all realistic, so we have developed a better way.

In this paper, we first consider an unregularized least-squares fitting problem that extracts the g_{ij} from the d_{ij} at multiple receivers. This corresponds to a multichannel deconvolution (Amari et al., 1997; Douglas et al., 1997; Sroubek and Flusser, 2003) of the cross-correlated records in eq. 1, with an unknown blurring kernel s_{a}. We label this problem as *interferometric* blind deconvolution (IBD) and demonstrate that it can only be solved up to an indeterminacy due to a real and non-negative filter in the frequency domain. Therefore, we add an additional constraint to the IBD framework to focus the energy near zero lag in the estimated g_{ii}. This constraint is then relaxed to enhance the data fit. We call the resulting algorithm focused blind deconvolution (FBD). It can effectively retrieve the g_{ij}, provided the following conditions are met:

1. the duration length of the unknown g_{ij} should be much briefer than that of the d_{ij};

2. *sufficiently dissimilar* receivers record the noise.

In the seismic imaging context, the first condition is very convenient, as usual drilling practice enables us to record noise for a time period much longer compared to the wave-propagation time. We show that the second condition can be satisfied in most practical situations. FBD is a mostly data-driven algorithm, in the sense that it doesn't require any velocity model or prior assumption on the noisy source, although it does apply a type of sparsity prior on the Green's functions.

Deconvolution is also an important step in the processing workflow used by exploration geophysicists to improve the resolution of the seismic sections (Ulrych et al., 1995; Liu and Liu, 2003; Van der Baan and Pham, 2008). Spiking deconvolution (Yilmaz, 2001) estimates a Wiener filter that increases the *whiteness* of the seismic records, therefore, removing the effect of the seismic sources. In blind deconvolution (BD*) the challenge is that the source signature is unknown. It is widely used for deblurring (Levin et al., 2011a,b), where an unknown blur kernel contaminates the visually plausible sharp image. Severe non-uniqueness issues are inherent to BD; there could be many possible g_i and s pairs whose convolution will result in the observed data. In order to alleviate these non-uniqueness issues, recent BD algorithms in geophysics: 1. take advantage of the multichannel nature of the seismic data (Kaaresen and Taxt, 1998; Kazemi and Sacchi, 2014; Nose-Filho et al., 2015; Liu et al., 2016); 2. sensibly choose the initial estimates of the g_i in order to converge to a desired solution (Liu et al., 2016);

---

and/or 3. constrain the sparsity of the g_i (Kazemi and Sacchi, 2014). Kazemi et al. (2016) used sparse multichannel BD to estimate source and receiver wavelets while processing land seismic data. The BD algorithms in the current geophysics literature handle roughly impulsive source wavelets that are due to well-controlled sources, as opposed to the noisy sources in FBD, about which we assume very little. It has to be observed that building initial estimates of the g_i is difficult for any algorithm, as the functional distances between the d_i and the actual g_i are quite large. Unlike standard methods, FBD does not require an extrinsic starting guess. Note also that regularization in the sense of minimal L^1 i.e., mean-absolute norm, as some methods employ, does not fully address the type of indeterminacy described below in eq. 8.

The failure of seismic noisy sources to be white[†] is already well known in seismic interferometry (Curtis et al., 2006; Vasconcelos and Snieder, 2008). To extract a building response, Snieder and Safak (2006) propose a deconvolution of the recorded waves at different locations in the building rather than the cross-correlation. Seismic interferometry by multi-dimensional deconvolution (Wapenaar et al., 2008, 2011; van der Neut et al., 2011; Broggini et al., 2014) uses an estimated interferometric point spread function as a deconvolution operator. The results obtained from this approach depend on the accuracy of the estimated point spread function, which relies on a uniform distribution of multiple noisy sources in space. In contrast to these seismic-interferometry-by-deconvolution approaches, our FBD is designed to perform a *blind* deconvolution in the presence of a single noisy source. The reflection-imaging experiments in this paper are similar to those of Tateno et al. (1998), Vidal et al. (2014), Boullenger et al. (2014) and Nishitsuji et al. (2016), except that we deal with a single noisy source at a known location. In the presence of multiple noisy sources, as a pre-process to FBD, one has to use techniques such as independent component analysis for deblending (Bharadwaj et al., 2017).

FOCUSED BLIND DECONVOLUTION

In this section, we will detail three different multichannel BD algorithms for a single seismic noisy source. The gist of these algorithms is a least-squares fitting of the (cross-correlated) d_i to jointly optimize two variables i.e., the (cross-correlated) g_i and the (auto-correlated) s. The joint optimizations in these algorithms can be suitably carried out using alternating minimization (Ayers and Dainty, 1988; Sroubek and Milanfar, 2012): in one cycle, we fix one variable and optimize the other, and then fix the other and optimize the first. Several cycles are expected to be performed to reach convergence. In order to effectively solve these problems, it is required that the length of the (cross-correlated) records at the receivers be longer than that of the unknown (cross-correlated) Green's functions (Ahmed et al., 2015; Ahmed and Demanet, 2016).

We denote the time domains of s and g_i by $\{t \mid 0 \le t \le T\}$ and $\{t \mid 0 \le t \le \tau\}$, respectively. Here, τ denotes the propagation time necessary for the seismic energy, including multiple scattering, traveling from the source to a total of n_r receivers, to decrease below an ad-hoc threshold. Approximating the Earth as a linear system, the recorded signals at the ith receiver are given by a convolution of the source signature with the Green's functions: $d_i(t) = [s * g_i](t)$. The data are measured only for

---

[†]For example, the noise generated by drill bit operations is heavily correlated in time (Rector III and Marion, 1991; Joyce et al., 2001).

$0 \le t \le T$, so we are not assuming that the source is turned off throughout that time interval, just as in usual drilling operations.

Definition 1 (LSBD: Least-squares Blind Deconvolution). It is the most basic formulation, where both the unknown $s(t)$ and the unknown $g_i(t)$ are estimated given the recorded data $d_i(t)$:

$$U(s, g_j) = \sum_i \sum_t \{d_i(t) - [s * g_i](t)\}^2; \qquad (2)$$

$$(\hat{s}, \hat{g}_i) = \operatorname*{arg\,min}_{s, g_i} \quad U \qquad (3)$$

$$\text{subject to} \quad \sum_t s^2(t) = 1.$$

We have fixed the energy (i.e., sum-of-squares) norm of s in order to resolve the scaling ambiguity. Note that the length T of the first unknown variable s has to be greater than the length τ of the second unknown variable g_i. Later in this section, we will discuss that the LSBD problem can only be solved up to some indeterminacy.

Definition 2 (IBD: Interferometric Blind Deconvolution). This reformulation deals with the cross-correlated records $d_{ij} : \{t \mid -T \le t \le T\} \to \mathbb{R}$ between every possible receiver pair (cf., Demanet and Jugnon, 2017). The optimization is carried out over $s_a : \{t \mid -T \le t \le T\} \to \mathbb{R}$ and $g_{ij} : \{t \mid -\tau \le t \le \tau\} \to \mathbb{R}$:

$$V(s_a, g_{ij}) = \sum_{i,j} \sum_t \{d_{ij}(t) - [s_a * g_{ij}](t)\}^2; \qquad (4)$$

$$(\hat{s}_a, \hat{g}_{ij}) = \operatorname*{arg\,min}_{s_a, g_{ij}} \quad V \qquad (5)$$

$$\text{subject to} \quad s_a(0) = 1.$$

During the minimization, we have conveniently fixed $s_a(0)$ in order to resolve the scaling ambiguity. IBD also requires $T > \tau$ and its indeterminacy is lesser compared to that of the LSBD approach.

Definition 3 (FBD: Focused Blind Deconvolution). FBD starts by seeking a solution of the underdetermined IBD problem where the Green's functions are "maximally white", as measured by the concentration of their autocorrelation near zero lag. Towards that end, we use a regularizing term that penalizes the energy of the autocorrelated Green's functions g_{ii} at non-zero lags, before returning to solving the regular IBD problem. This prescription does not guarantee that the recovered interferometric Green's functions are physical:

$$W(s_a, g_{ij}) = V(s_a, g_{ij}) + \alpha \sum_i \sum_t \frac{|t|}{\tau} g_{ii}^2(t); \qquad (6)$$

$$(\hat{s}_a, \hat{g}_{ij}) = \operatorname*{arg\,min}_{s_a, g_{ij}} \quad W \qquad (7)$$

$$\text{subject to} \quad s_a(0) = 1.$$

Here, $\alpha > 0$ is a regularization parameter. We consider a homotopy (Osborne et al., 2000) approach to solve FBD, where eq. 7 is solved in succession for decreasing values of α, the result obtained for previous α being used as an initializer for the cycle that uses the current α. In the numerical examples, we simply choose $\alpha = \infty$ first, and then $\alpha = 0$.

Ill-posedness is the major challenge of BD, irrespective of the number of receivers. For instance, when $n_r = 1$, an undesirable minimizer for eqs. 2, 4 & 6 would be the Kronecker delta for the second variable at the receiver, making the first variable equal the record vector. To quantify the ambiguity of the LSBD formulation, when $n_r \ge 1$, consider that a filter $\phi(t)$ and its inverse $\phi^{-1}(t)$ (where $\phi * \phi^{-1} = \delta$) can be applied to s and g_i

respectively, and leave their convolution unchanged:

$$d_i(t) = [s * g_i](t) = \{[s * \phi] * [g_i * \phi^{-1}]\}(t). \tag{8}$$

If furthermore $s * \phi$ and $g_i * \phi^{-1}$ obey the constraints otherwise placed on s and g_i, namely in our case that g_i should be supported on $0 \leq t \leq \tau$, then we are in presence of a true ambiguity not resolved by those constraints. We then speak of ϕ as belonging to a set $\mathbb{P}$ of undetermined filters (other than the identity). This formalizes the lack of uniqueness: For every $\phi \in \mathbb{P}$, $(\hat{s} * \phi, \hat{g}_i * \phi^{-1})$ is an additional possibly undesirable solution that minimizes the least-squares functional in eq. 2, resulting in non-uniqueness. Note that the indeterminacy, quantified by $|\mathbb{P}|$, reduces with increase in n_r.

In the case of IBD, eq. 4 has similar unwanted minimizers, obtained by applying a filter Φ to s_a and Φ^{-1} to g_{ij}, but it is easily computed that in the frequency domain $\bar{\Phi}$ has to be *real and nonnegative*. The set of filters $\mathbb{P}$ is now much smaller than in the case of LSBD, hence the indeterminacy is greatly reduced in the case of IBD.

The FBD approach uses the focusing constraint, as in eq. 6, to resolve the remaining indeterminacy of IBD. Minimizing the energy of the auto-correlated Green's functions g_{ii} at non-zero lags will result in a solution where the Green's functions are heuristically as white as possible. In other words, the intention and key innovation of FBD is that the undetermined filter Φ, which tends to have finite impulse response, is pushed onto the source term s_a as much as possible, where it is less harmful than on the sparse g_{ij}. It is difficult to achieve the same result with standard ideas from sparse regularization.

For the success of FBD, it is also important that the receivers and their data are *sufficiently dissimilar*. Receivers are said to be *sufficiently dissimilar* unless there exists a spurious $\gamma \in \mathbb{P}$ and functions g_{ij} such that the true interferometric Green's function $g_{ij}^0 = \gamma * g_{ij}$. Here, γ is a real and nonnegative filter in the frequency domain (nontrivial in the sense that it is not completely frequency-independent), independent of the receiver index i, that causes indeterminacy of the IBD problem. In our experiments, FBD reconstructs a good approximation of the true interferometric Green's functions if the receivers are sufficiently dissimilar. Otherwise, FBD outputs an undesirable solution $(s_a^0 * \gamma, g_{ij})$, as opposed to the true solution $(s_a^0, \gamma * g_{ij})$, where s_a^0 is the true auto-correlated source signature. In the next section, we will show numerical examples with both similar and dissimilar receivers for a subsurface model with single reflector.

IMAGING USING DRILL-BIT NOISE

The seismic-while-drilling experiments in this section, with homogeneous velocity $c_p = 2.9$ km/s, are classified into three scenarios that assume acoustic subsurface models. The goal of these experiments is to reconstruct the subsurface interferometric Green's functions g_{ij} that contain: 1. the direct arrival from the drill bit to the drill-string receivers — useful for determination of the background velocity; and 2. the scattered waves from either horizontal or vertical reflectors due to a mass-density contrast — necessary for imaging. The mass-density models are shown in the Figures 1a–1c, where the drill bit and ten receivers, evenly spaced roughly 8 m apart on either a vertical or horizontal bore hole, are also marked. We used an acoustic time-domain staggered-grid finite-difference solver for wave-equation modeling. To generate the 'observed' data d_i, a band-limited correlated drill-bit signal is injected for $T = 2$ s. The sig-
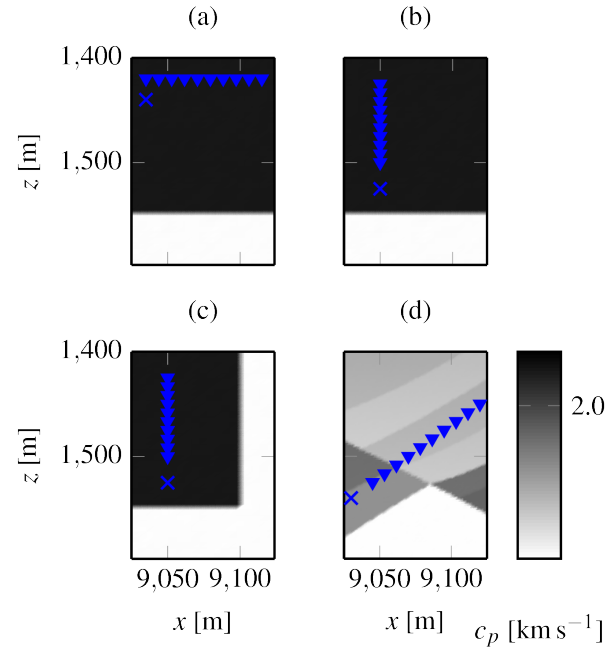

Figure 1: Subsurface models used for drill-bit-noise numerical experiments. a) Seismic impedance model with a horizontal reflector and dissimilar receivers for FBD. b) Same as (a), but with similar receivers. c) Model with two reflectors resulting in strong multiple scattering. c) A section of the Marmousi II P-wave velocity model with a deviated well.
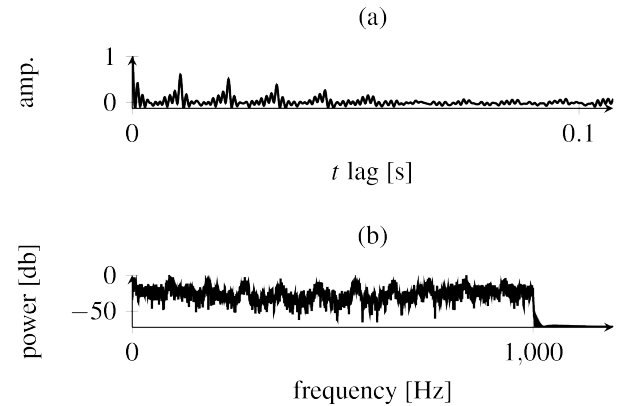

Figure 2: For the drill-bit source used in the synthetic experiments: (a) auto-correlation that contaminates the interferometric Green's functions in the time domain — only 1% of T is plotted; (b) power spectrum.

nal's auto-correlation and power spectrum are plotted in the Figures 2a and 2b, respectively. The 'true' interferometric Green's functions g_{ij}^0 in Figures 3c, 3f and 3i, which we aim to reconstruct, are generated following these steps: 1. get data for $\tau = 0.1$ s using a Ricker source wavelet (peak frequency of 400 Hz); 2. create cross-correlated data; and 3. perform a deterministic deconvolution on the cross-correlated data using the power spectrum of the Ricker wavelet. Observe that we have chosen the propagation time to be $\tau = 0.1$ s, such that $T/\tau = 20$.

In all three scenarios, the drill bit's auto-correlation contaminates the cross-correlated data d_{ij}, as plotted in Figures 3a, 3d and 3g, which prevents extraction of both the direct and the scattered arrivals of the true interferometric Green's functions.
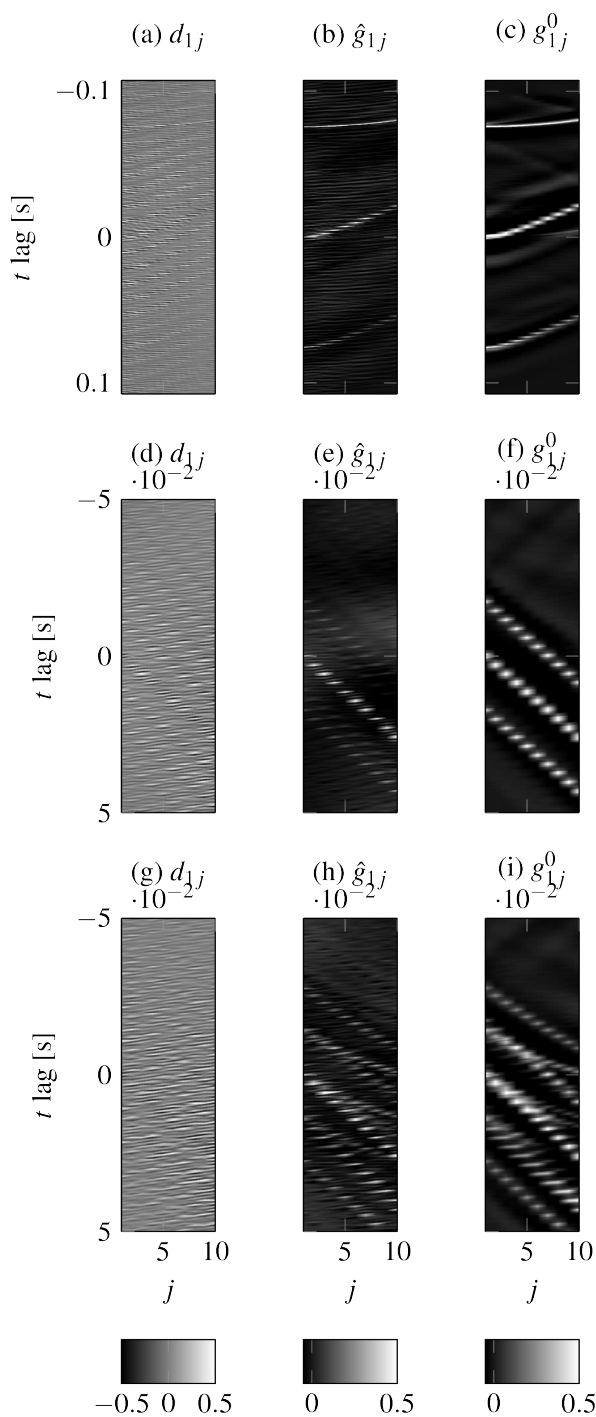
Figure 3: FBD results corresponding to the seismic-while-drilling experiments in: a)—c) Figure 1a; d)—f) Figure 1b; g)—i) Figure 1c.
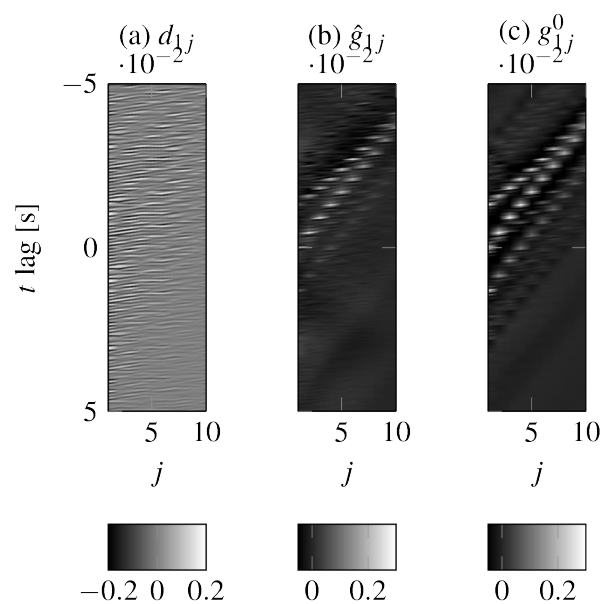

Figure 4: FBD for the Marmousi experiment in Figure 1d.

reflectors; as an example, we look at the results using the third-scenario model with two reflectors. FBD satisfactorily recovers the interferometric Green's functions, as plotted in Figure 3h, even when there is multiple scattering due to two strong reflectors.

Finally, we consider a more realistic scenario with a section of the Marmousi c_p model in Figure 1d and a deviated well. The parameters for this scenario are the same as that of the previous scenarios. The results in Figure 4 confirm that FBD doesn't suffer from the complexities in the subsurface models.

CONCLUSIONS

Focused blind deconvolution (FBD) extracts the interferometric Green's functions by least-squares fitting of the cross-correlated records due to a single noisy source that can be a drill bit with noise whose temporal correlations would stymie traditional methods. FBD focuses the energy of the auto-correlated Green's functions at the zero lag before aiming for an improved data fit. It is a mostly data-driven algorithm that doesn't demand any velocity-model or noisy-source assumptions, designed for an acquisition with longer record time (e.g., from normally scheduled drilling operations) than the wave-propagation time. We have demonstrated the benefits of FBD using seismic-while-drilling experiments to look around and ahead of a bore-hole. FBD doesn't guarantee that the recovered interferometric Green's functions are physical.

ACKNOWLEDGEMENTS

In the case of the first scenario, FBD results in a favorable outcome $\hat{g}_{ij}$, as plotted in Figure 3b, because the receivers are sufficiently dissimilar. For the second scenario, the FBD outcome in Figure 3e doesn't clearly depict the scattered arrivals because of the receiver similarity, corresponding to the reflector being parallel to the line of receiver positions. In this regard, observe that the Figure-3f true interferometric Green's functions at various receiver indices j differ only by a fixed time-translation instead of curving as in Figure 3c. In fact, the receiver positions in the second scenario are probably sufficiently dissimilar for any other subsurface model than the one with *only* horizontal

REFERENCES

Ahmed, A., A. Cosse, and L. Demanet, 2015, A convex approach to blind deconvolution with diverse inputs: Computational Advancesin Multi-Sensor Adaptive Processing (CAMSAP), IEEE 6th International Workshop on, IEEE, 5–8.

Ahmed, A., and L. Demanet, 2016, Leveraging diversity and sparsity in blind deconvolution: arXiv preprint arXiv:1610.06098.

Amari, S.-i., S. C. Douglas, A. Cichocki, and H. H. Yang, 1997, Multichannel blind deconvolution and equalization using the natural gradient: Signal Processing Advances in Wireless Communications, First IEEE Signal Processing Workshop on, IEEE, 101–104.

Aminzadeh, F., and S. N. Dasgupta, 2013, Geophysics for petroleum engineers. Newnes 60.

Ayers, G., and J. C. Dainty, 1988, Iterative blind deconvolution method and its applications: Optics Letters, **13**, 547–549.

Bharadwaj, P., L. Demanet, and A. Fournier 2017, Deblending random seismic sources via independent component analysis: Presented at the 87th Annual International Meeting, SEG.

Borcea, L., G. Papanicolaou, and C. Tsogka, 2006, Coherent interferometric imaging in clutter: Geophysics, **71**, no. 4, SI165–SI175, https://doi.org/10.1190/1.2209541.

Boullenger, B., A. Verdel, B. Paap, J. Thorbecke, and D. Draganov, 2014, Studying CO_2 storage with ambient-noise seismic interferometry: A combined numerical feasibility study and field-data example for Ketzin, Germany: Geophysics, **80**, no. 1, Q1–Q13, https://doi.org/10.1190/geo2014-0181.1.

Broggini, F., R. Snieder, and K. Wapenaar, 2014, Data-driven wavefield focusing and imaging with multidimensional deconvolution: Numerical examples for reflection data with internal multiples: Geophysics, **79**, no. 3, WA107–WA115, https://doi.org/10.1190/geo2013-0307.1.

Campisi, P., and K. Egiazarian, 2016, Blind image deconvolution: Theory and applications: CRC press.

Claerbout, J. F., 1968, Synthesis of a layered medium from its acoustic transmission response: Geophysics, **33**, 264–269, https://doi.org/10.1190/1.1439927.

Curtis, A., P. Gerstoft, H. Sato, R. Snieder, and K. Wapenaar, 2006, Seismic interferometry — turning noise into signal: The Leading Edge, **25**, 1082–1092.

Demanet, L., and V. Jugnon, 2017, Convex recovery from interferometric measurements: IEEE Transactions on Computational Imaging, **3**, 282–295.

Douglas, S. C., A. Cichocki, and S.-I. Amari, 1997, Multichannel blind separation and deconvolution of sources with arbitrary distributions: Neural Networks for Signal Processing VII. Proceedings of the 1997 IEEE Workshop, IEEE, 436–445.

Draganov, D., K. Wapenaar, and J. Thorbecke, 2006, Seismic interferometry: Reconstructing the earth's reflection response: Geophysics, **71**, no. 4, SI61–SI70, https://doi.org/10.1190/1.2209947.

Haldorsen, J. B., D. E. Miller, and J. J. Walsh, 1995, Walk-away VSP using drill noise as a source: Geophysics, **60**, 978–997, https://doi.org/10.1190/1.1443863.

Joyce, B., D. Patterson, J. Leggett, and V. Dubinsky, 2001, Introduction of a new omni-directional acoustic system for improved real-time LWD sonic logging-tool design and field test results: Presented at the SPWLA 42nd Annual Logging Symposium, SPWLA.

Kaaresen, K. F., and T. Taxt, 1998, Multichannel blind deconvolution of seismic signals: Geophysics, **63**, 2093–2107, https://doi.org/10.1190/1.1444503.

Kazemi, N., E. Bongajum, and M. D. Sacchi, 2016, Surface-consistent sparse multichannel blind deconvolution of seismic signals: IEEE Transactions on Geoscience and Remote Sensing, **54**, 3200–3207, https://doi.org/10.1109/TGRS.2015.2513417.

Kazemi, N., and M. D. Sacchi, 2014, Sparse multichannel blind deconvolution: Geophysics, **79**, no. 5, V143–V152, https://doi.org/10.1190/geo2013-0465.1.

Kundur, D., and D. Hatzinakos, 1996, Blind image deconvolution: IEEE Signal Processing Magazine, **13**, 43–64.

Levin, A., Y. Weiss, F. Durand, and W. T. Freeman, 2011a, Efficient marginal likelihood optimization in blind deconvolution: IEEE Conference on Computer Vision and Pattern Recognition, 2657–2664.

Levin, A., Y. Weiss, F. Durand, and W. T. Freeman, 2011b, Understanding blind deconvolution algorithms: IEEE Transactions on Pattern Analysis and Machine Intelligence, **33**, 2354–2367, https://doi.org/10.1109/TPAMI.2011.148.

Liu, E., N. Iqbal, J. H. McClellan, and A. A. Al-Shuhail, 2016, Sparse blind deconvolution of seismic data via spectral projected-gradient: arXiv preprint arXiv:1611.03754.

Liu, X., and H. Liu, 2003, Survey on seismic blind deconvolution: Progress in Geophysics, **18**, 203–209.

Nishitsuji, Y., S. Minato, B. Boullenger, M. Gomez, K. Wapenaar, and D. Draganov, 2016, Crustal-scale reflection imaging and interpretation by passive seismic interferometry using local earthquakes: Interpretation, **4**, SJ29–SJ53.

Nose-Filho, K., A. K. Takahata, R. Lopes, and J. M. Romano, 2015, A fast algorithm for sparse multichannel blind deconvolution: Geophysics, **81**, no. 1, V7–V16, https://doi.org/10.1190/geo2015-0069.1.

Osborne, M. R., B. Presnell, and B. A. Turlach, 2000, A new approach to variable selection in least squares problems: IMA Journal of Numerical Analysis, **20**, 389–403, https://doi.org/10.1093/imanum/20.3.389.

Rector III, J., and B. P. Marion, 1991, The use of drill-bit energy as a downhole seismic source: Geophysics, **56**, 628–634, https://doi.org/10.1190/1.1443079.

Robinson, E. A., and S. Treitel, 1980, Geophysical signal analysis: Prentice-Hall Englewood Cliffs 263.

Schuster, G., J. Yu, J. Sheng, and J. Rickett, 2004, Interferometric/daylight seismic imaging: Geophysical Journal International, **157**, 838–852.

Schuster, G. T., 2009, Seismic interferometry: Cambridge University Press 1.

Shapiro, N. M., M. Campillo, L. Stehly, and M. H. Ritzwoller, 2005, High-resolution surface-wave tomography from ambient seismic noise: Science, **307**, 1615–1618.

Snieder, R., 2004, Extracting the green's function from the correlation of coda waves. A derivation based on stationary phase: Physical Review E, **69**, 046610, https://doi.org/10.1103/PhysRevE.69.046610

Snieder, R., and E. Safak, 2006, Extracting the building response using seismic interferometry. Theory and application to the Millikan Library in Pasadena, California: Bulletin of the Seismological Society of America, **96**, 586–598, https://doi.org/10.1785/0120050109

Sroubek, F., and J. Flusser, 2003, Multichannel blind iterative image restoration: IEEE Transactions on Image Processing, **12**, 1094–1106, https://doi.org/10.1109/TIP.2003.815260

Sroubek, F., and P. Milanfar, 2012, Robust multichannel blind deconvolution via fast alternating minimization: IEEE Transactions on Image Processing, **21**, 1687–1700.

Tateno, M., M. Takahashi, I. Suzuki, K. Akaku, T. Uchida, H. Niitsuma, and H. Asanuma, 1998, Estimation of deep reflectors using triaxial drill bit vsp in nedo deep-seated geothermal resources survey, Kakkonda, Japan: Geothermics, **27**, 647–661.

Ulrych, T. J., D. R. Velis, and M. D. Sacchi, 1995, Wavelet estimation revisited: The Leading Edge, **14**, 1139–1143.

Van der Baan, M., and D.-T. Pham, 2008, Robust wavelet estimation and blind deconvolution of noisy surface seismics: Geophysics, **73**, no. 5, V37–V46, https://doi.org/10.1190/1.2965028

Van der Neut, J., J. Thorbecke, K. Mehta, E. Slob, and K. Wapenaar, 2011, Controlled-source interferometric redatuming by cross-correlation and multidimensional deconvolution in elastic media: Geophysics, **76**, no. 4, SA63–SA76, https://doi.org/10.1190/1.3580633

Vasconcelos, I., and R. Snieder, 2008, Interferometry by deconvolution: Part 1 — Theory for acoustic waves and numerical examples: Geophysics, **73**, no. 3, S115–S128, https://doi.org/10.1190/1.2904554

Vidal, C. A., D. Draganov, J. Van der Neut, G. Drijkoningen, and K. Wapenaar, 2014. Retrieval of reflections from ambient noise using illumination diagnosis: Geophysical Journal International, **198**, 1572–1584.

Wapenaar, K., and J. Fokkema, 2006, Green's function representations for seismic interferometry: Geophysics, **71**, no. 4, SI33–SI46, https://doi.org/10.1190/1.2213955

Wapenaar, K., E. Slob, and R. Snieder, 2006, Unified green's function retrieval by cross correlation: Physical Review Letters, **97**, 234301.

Wapenaar, K., J. van der Neut, and E. Ruigrok, 2008, Passive seismic interferometry by multidimensional deconvolution: Geophysics, **73**, no. 6, A51–A56, https://doi.org/10.1190/1.2976118

Wapenaar, K., J. Van Der Neut, E. Ruigrok, D. Draganov, J. Hunziker, E. Slob, J. Thorbecke, and R. Snieder, 2011. Seismic interferometry by crosscorrelation and by multidimensional deconvolution: A systematic comparison: Geophysical Journal International, **185**, 1335–1364, https://doi.org/10.1111/j.1365-246X.2011.05007.x

Yilmaz, Ö., 2001, Seismic data analysis: SEG 1.